Mutation for non-syndromic mental retardation in the *trans*-2-enoyl-CoA reductase *TER* gene involved in fatty acid elongation impairs the enzyme activity and stability leading to change in sphingolipid profile*

Kensuke Abe[1], Yusuke Ohno[1], Takayuki Sassa[1], Ryo Taguchi[2], Minal Çalışkan[3], Carole Ober[3], Akio Kihara[1]

[1]From Laboratory of Biochemistry, Faculty of Pharmaceutical Sciences, Hokkaido University, Kita 12-jo, Nishi 6-chome, Kita-ku, Sapporo 060-0812, Japan

[2]Department of Biomedical Sciences, College of Life and Health Sciences, Chubu University, 1200 Matsumoto-cho, Kasugai 487-8501, Japan

[3]Department of Human Genetics, University of Chicago, 920 E. 58th Street, Chicago, IL 60637, USA

*Running title: *Reduced activity and stability of TER P182L mutant enzyme*

To whom correspondence should be addressed: Akio Kihara, Faculty of Pharmaceutical Sciences, Hokkaido University, Kita 12-jo Nishi 6-chome, Kita-ku, Sapporo 062-0812, Japan, Tel.: +81-11-706-3754; Fax: +81-11-706-4900; E-mail: kihara@pharm.hokudai.ac.jp

Keywords: fatty acid; fatty acid metabolism; lipids; membrane; sphingolipid

Background: The *P182L* mutation in the *trans*-2-enoyl-CoA reductase *(TER*) gene required for very long-chain fatty acid (VLCFA) synthesis causes non-syndromic mental retardation.
Results: This mutation reduces the activity and stability of the TER enzyme.
Conclusion: The impaired TER function affects VLCFA synthesis and thereby alters the cellular sphingolipid profile.
Significance: Maintenance of a proper VLCFA level may be important for neural function.

SUMMARY

Very long-chain fatty acids (VLCFAs, chain length >C20) exist in tissues throughout the body and are synthesized by repetition of the fatty acid (FA) elongation cycle composed of four successive enzymatic reactions. In mammals, the *TER* gene is the only gene encoding *trans*-2-enoyl-CoA reductase, which catalyzes the fourth reaction in the FA elongation cycle. The *TER P182L* mutation is the pathogenic mutation for non-syndromic mental retardation (NSMR). This mutation substitutes a leucine for a proline residue at amino acid 182 in the TER enzyme. Currently, the mechanism by which the *TER P182L* mutation causes NSMR is unknown. In order to understand the effect of this mutation on the TER enzyme and VLCFA synthesis, we have biochemically characterized the TER P182L mutant enzyme using yeast and mammalian cells transfected with the *TER P182L* mutant gene and analyzed the FA elongation cycle in the B-lymphoblastoid cell line with the homozygous *TER P182L* mutation (*TER*$^{P182L/P182L}$ B-LCL). We have found that TER P182L mutant enzyme exhibits reduced *trans*-2-enoyl-CoA reductase activity and protein stability, thereby, impairing VLCFA synthesis and, in turn, altering the sphingolipid profile (*i.e.*, decreased level of C24 sphingomyelin and C24 ceramide) in the *TER*$^{P182L/P182L}$ B-LCL. We have also found that in addition to the TER enzyme-catalyzed fourth reaction, the third reaction in the FA elongation cycle is affected by the *TER P182L* mutation. These findings provide new insight into the biochemical defects associated with this genetic mutation.

Very long-chain fatty acids (VLCFAs) are fatty acids (FAs) with a carbon chain greater than twenty carbons (>C20). A variety of VLCFAs, differing in their chain lengths (up to C40) and degree of saturation (saturated, monounsaturated, n-3/n-6 polyunsaturated) have been reported in mammalian tissues (1-3).

Although much less abundant than long-chain (C11-C20) FAs (LCFAs), VLCFAs are ubiquitous among tissues and play an important function that cannot be substituted for by LCFAs, including skin barrier formation, neural function, retina function, and resolution of inflammation (1-3).

VLCFAs are synthesized in the endoplasmic reticulum (ER) from dietary or endogenous LCFAs by the sequential addition of two-carbon units from malonyl-CoA (Fig. 1*A*). Each elongation cycle is composed of four reactions catalyzed by distinct enzymes (2,3): [1] condensation of an acyl-CoA substrate and malonyl-CoA by FA elongase to form 3-ketoacyl-CoA, which is the rate-limiting step of the elongation cycle (4); [2] reduction of the 3-keto group to a 3-hydroxyl group by NADPH-dependent 3-ketoacyl-CoA reductase; [3] dehydration of the resulting 3-hydroxyacyl-CoA to *trans*-2-enoyl-CoA by 3-hydroxyacyl-CoA dehydratase; and [4] reduction of the *trans*-2 double bond by NADPH-dependent *trans*-2-enoyl-CoA reductase yielding the elongated acyl-CoA. Currently, there are seven FA elongases with characteristic substrate specificities and tissue expression patterns (ELOVL1-7) (5), one 3-ketoacyl-CoA reductase (KAR) (6), four 3-hydroxyacyl-CoA dehydratases (HACD1-4) (7), and one *trans*-2-enoyl-CoA reductase (TER/TECR/GPSN2) (6) known in mammals.

Most of the saturated and monounsaturated VLCFAs synthesized in the ER are used for sphingolipid synthesis (3). Sphingolipids are one of the major membrane lipids in eukaryotes and consist of a ceramide backbone (*i.e.*, a long-chain base with an amide-linked FA) and a polar head group (8). The polar head group of mammalian sphingolipids is either phosphocholine in sphingomyelin or a sugar chain in glycosphingolipids (8,9). The simplest glycosphingolipids are hexosylceramides, including glucosylceramide and galactosylceramide, the latter of which and its sulfated derivative (sulfatide) are abundant in myelin (10). Sphingolipids containing VLCFAs (mainly C24:0 and C24:1) are ubiquitous among mammalian tissues and are especially abundant in the liver, kidney, and brain (3,11,12). For example, C24 sphingomyelin constitutes ~60% of the total sphingomyelin in the liver (11), and C24 galactosylceramide/sulfatide constitutes ~70% of the total galactosylceramide/sulfatide in the spinal cord (12).

Impairment of VLCFA synthesis is associated with several disorders and dysfunctions (3). For example, the dominant mutation in the *ELOVL4* gene causes Stargardt disease type 3, which is a juvenile-onset macular dystrophy (13), whereas the recessive *ELOVL4* mutation leads to a neurocutaneous disorder of ichthyosis, seizures, mental retardation, and spasticity (14). A recessive mutation in the 3-hydroxyacyl-CoA dehydratase *HACD1*/*PTPLA* gene of the dog (15) and human (16) is known to cause myopathy. Moreover, VLCFAs have been shown to be essential for viability of yeast and mammals; for example, deletion of the *TSC13* gene (the only yeast *trans*-2-enoyl-CoA reductase gene, *i.e.*, the yeast homolog of the *TER* gene) is lethal in yeast (17), and likewise the only 3-ketoacyl-CoA reductase *KAR* gene knockout mice result in embryonic lethality due to disruption of organogenesis (18).

Recently, the *P182L* mutation in the *TER* gene (*TER P182L* mutation) has been identified in patients with non-syndromic mental retardation (NSMR) (19). This mutation causes a substitution of a leucine for a proline residue at residue 182 in the TER enzyme (Fig. 1*B*). Although the membrane topology of the mammalian TER enzyme has not been determined, it is highly likely that this enzyme is an integral membrane protein with six membrane spanning domains and cytosolic N- and C-termini (Fig. 1*C*) as deduced from the membrane topology of the yeast and *Arabidopsis* TER homologs (20). In this topology model, the Pro182 residue is positioned in the second luminal loop.

Like the KAR enzyme, which is the only mammalian 3-ketoacyl-CoA reductase involved in VLCFA synthesis and is essential for embryonic viability (18), the TER enzyme is the only isoform of mammalian *trans*-2-enoyl-CoA reductase for VLCFA synthesis; therefore, the *TER* null mutation should also be considered to be embryonically lethal. Since the *TER P182L* mutation affects only mental development (19),

the TER P182L mutant enzyme appears to retain some residual function. The *TER P182L* mutation, not being a null mutation, must be useful for understanding the function of VLCFA in various tissues. In the present study, we have investigated the effect of the *P182L* mutation on the activity, stability, and intracellular localization of the TER enzyme using yeast and mammalian cells transfected with the *TER P182L* mutant gene. We have also analyzed the FA elongation cycle in the B-lymphoblastoid cell line (B-LCL) derived from NSMR patients (homozygous for the *TER P182L* mutation, $TER^{P182L/P182L}$) to gain some insight into the pathogenesis of NSMR.

EXPERIMENTAL PROCEDURES

Cell culture and transfection — HEK 293T and HeLa cells were grown in DMEM (D6429 for HEK 293T cells and D6046 for HeLa cells; Sigma, St. Louis, MO) supplemented with 10% FBS, 100 units/ml penicillin, and 100 μg/ml streptomycin; HEK 293T cells were maintained in dishes coated with 0.3% collagen. Transfections were performed using Lipofectamine Plus™ Reagent (Life Technologies, Carlsbad, CA) according to the manufacturer's instructions.

B-LCLs were generated at the University of Chicago from four NSMR patients, four carriers, and three non-carrier healthy controls. This study was approved by the Institutional Review Board at the University of Chicago. All unaffected subjects provided written informed consent; informed consents were obtained from the parents of the NSMR patients. Peripheral blood mononuclear cells were isolated from whole blood samples of each subject using Ficoll-Paque separation protocol (21). Peripheral blood mononuclear cells were then suspended in RPMI 1640 (Life Technologies) medium (supplemented with 20% fetal bovine serum and 50 μg/ml gentamicin) and incubated with Epstein–Barr virus at 37 ˚C and 5% CO_2 for 3-5 days to establish B-LCLs.

Plasmids — The pCE-puro 3xFLAG-1 plasmid is mammalian expression vector designed to produce a protein tagged with an N-terminal 3xFLAG (7). The pCE-puro 3xFLAG-TER plasmid was described previously (5). The pCE-puro 3xFLAG-TER P182L plasmid was constructed using QuikChange site-directed mutagenesis kit (Stratagene, Agilent Technologies, La Jolla, CA) with primers 5'-TATTACATCAATCACCTTCTCTACACTC CCCCT-3' and 5'-AGGGGGAGTGTAGAGAAGGTGATTGA TGTAATA-3'. The pAKNF314 (*GAPDH* promoter, *TRP1* marker), pAKNF313 (*GAPDH* promoter, *HIS3* marker), and pAK1172 (*ADH* promoter, *HIS3* marker) plasmids are yeast expression vectors each designed to produce an N-terminal 3xFLAG-tagged protein. The pAB85 (pAKNF314-*TER*), pAB114 (pAK1172-*TER*), pAB95 (pAKNF314-*TER P182L*), or pAB110 (pAKNF313-*TER P182L*) plasmid was constructed by cloning the *TER* or *TER P182L* cDNA into each vector.

Yeast strains and media — The yeast *Saccharomyces cerevisiae* strains used in this study were derived either from BY4741 (*MAT**a** his3Δ1 leu2Δ0 met15Δ0 ura3Δ0*) (22) or BY25598 *(MAT**a** his3-11,15 leu2-3,112 ura3::P_{ADH}-OsTIR1* (*URA3*) *trp1-1 ade2-1 can1-100*) (23). YRF82 cells (*TSC13-HA-AID*) were constructed by chromosomal fusion of a coding sequence for tandemly oriented HA and auxin-inducible degron (AID) with the *TSC13* gene from BY25598 cells as described previously (24). For construction of ABY58 (BY4741, *tsc13Δ::LEU2*/pAB110) and ABY62 (BY4741, *tsc13Δ::LEU2*/pAB114) cells, the pAB110 (*3xFLAG-TER P182L*) and pAB114 (*3xFLAG-TER*) plasmids were respectively introduced into BY4741 cells. The *tsc13Δ::LEU2* mutation was then introduced into each of the resultant cells. Cells were grown in synthetic complete (SC) medium (0.67% yeast nitrogen base, 2% D-glucose, and nutritional supplements) without Trp (SC-Trp) or His (SC-His) at 30 ˚C.

In vitro trans-2-enoyl-CoA reductase assay — The yeast membrane fraction was prepared as follows: yeast cells suspended in buffer I (50 mM HEPES-NaOH (pH 6.8), 150 mM NaCl, 10% glycerol, 1 mM DTT, 1 mM PMSF, and a 1X Complete™ protease inhibitor mixture

(EDTA-free; Roche Diagnostics, Indianapolis, IN)) were lysed by vigorous mixing with glass beads; unlysed cells were removed by centrifugation at 2,000 x g for 3 min; the supernatant was centrifuged at 100,000 x g and 4 ˚C for 30 min; and the resulting pellet (total membrane fraction) was suspended in buffer I.

The membrane fraction of B-LCLs was prepared as follows: cells were washed with PBS, suspended in buffer I, and lysed by sonication; cell debris was removed by centrifugation at 300 x g for 5 min; and the supernatant was centrifuged at 100,000 x g and 4 ˚C for 30 min; and the pellet (total membrane fraction) was suspended in buffer I.

The assay was performed by incubating the membrane fraction with 5 nCi 3-hydroxy[1-^{14}C]palmitoyl-CoA (55 mCi/mmol; American Radiolabeled Chemicals, St. Louis, MO) in 50 μl reaction buffer (buffer I containing 2 mM $MgCl_2$, 1 mM $CaCl_2$, and 1 mM NADPH) at 37 ˚C for 30 min. The reaction was terminated by adding 25 μl 75% (w/v) KOH-H_2O and 50 μl ethanol followed by heating at 70˚C for 1 h, and then the mixture was acidified with 100 μl 5 M HCl in 50 μl ethanol. Lipids were extracted with 700 μl hexane and dried. The lipid residue was suspended in 20 μl chloroform and separated by TLC on a Silica Gel 60 high performance TLC plate (Merck, Whitestation, NJ) with hexane/diethyl ether/acetic acid (30:70:1, v/v) as the solvent system. Radiolabeled lipids were detected by autoradiography and quantified by a bioimaging analyzer BAS-2500 (Fuji Photo Film, Tokyo, Japan).

In vitro FA elongation assay — The assay was performed as described previously (5) using 20 μg membrane fraction, 20 μM palmitoyl-CoA (Sigma), and [2-^{14}C]malonyl-CoA (55 mCi/mmol, American Radiolabeled Chemicals).

Immunological assays — Immunoblotting was performed as described previously (25) using the anti-FLAG antibody M2 (1 μg/ml; Stratagene), the anti-HA antibody 16B12 (1/1000 dilution; Covance, Princeton, NJ), the anti-Pma1 antibody yN-20 (0.4 μg/ml; Santa Cruz Biotechnology, Santa Cruz, CA), anti-Pgk1 antibody (1/2000 dilution; Life Technologies), or anti-α-tubulin antibody (1/1000, Sigma) as the primary antibody, together with HRP-conjugated anti-mouse or anti-goat IgG F(ab')$_2$ fragment (each at 1:7500 dilution; GE Healthcare Life Sciences, Buckinghamshire, UK) as the secondary antibody. The signal was detected with Pierce Western Blotting Substrate (Thermo Fisher Scientific, Waltham, MA).

Indirect immunofluorescence microscopy was performed as described previously (26) using the anti-FLAG antibody M2 (0.5 μg/ml, Stratagene), anti-calreticulin antibody (1/400 dilution; Alexis, Lausen, Switzerland), and DAPI stain (1 μg/ml; Roche Diagnostics, Indianapolis, IN). Fluorescence was observed under a DM5000B fluorescence microscope (Leica Microsystems, Wetzlar, Germany).

RT-PCR — The total RNA was isolated from B-LCLs using NucleoSpin RNA II kit (MACHERY-NAGEL, Dueren, Germany). RT-PCR was performed using SuperScript One-Step RT-PCR with Platinum Taq (Life Technologies) and the following primers: for *TER*, 5'-TTCAGAGCAGGAAGGGGATGATGGGC-3' and 5'-GTCACTCATTCCACTACATCAAGCG-3', and for *GAPDH*, 5'-CCAAGGTCATCCATGACAACTTTGG-3' and 5'-GGTCCACCACCCTGTTGCTGTAGCC-3'.

Pulse-chase experiment — HEK 293T cells were transfected with the pCE-puro 3xFLAG-TER or pCE-puro 3xFLAG-TER P182L plasmid. Forty-eight hours after transfection, the medium was changed to Cys/Met- and serum-free DMEM (D0422, Sigma). Cells were treated with 55 μCi [^{35}S]Met/[^{35}S]Cys (EXPRE^{35}S^{35}S protein labeling mix; PerkinElmer Life Sciences, Ontario, Canada) for 1 h. After changing the medium to normal DMEM medium (D6429, Sigma) containing 10% FCS, cells were incubated at 37˚C for 1, 2, 4, and 8 h. At the end of each incubation time, cells were washed with PBS, resuspended in 1 ml RIPA buffer prepared in-house (50 mM Tris-HCl (pH 8.0), 150 mM NaCl, 1 mM EDTA, 1% Triton X-100, 0.1%

SDS, 0.1% sodium deoxycholate, 1 mM DTT, 1 mM PMSF, and 1X Complete™ protease inhibitor mixture), and disrupted by five passages through a 21G needle. Cell debris was removed by centrifugation at 20,000 x g and 4˚C for 5 min, and the supernatant was incubated at 4 ˚C overnight with anti-FLAG M2 agarose beads (Sigma). The beads were washed twice with 1 ml RIPA buffer and once with 1 ml 10 mM Tris-HCl (pH 8.0), and the bound protein was eluted with 2x SDS sample buffer.

Lipid analysis using mass spectrometry (MS)— Cells were spiked with an internal standard, C17:0 sphingomyelin or C17:0 ceramide (500 pmol; Avanti Polar Lipids, Alabaster, AL), and homogenized in 250 µl chloroform/methanol (1:2, v/v). Extracted lipids were recovered by centrifugation at 9,000 x g and room temperature for 1 min and treated with 10 µl 4 M KOH in methanol. After incubation at 37 ˚C for 1 h, the mixture was neutralized with 10 µl 12 M formic acid and subjected to phase separation by adding 80 µl H_2O and 80 µl chloroform, followed by centrifugation. The organic phase was recovered and dried, and the lipid residue was suspended in chloroform/methanol (1:2, v/v). Lipids were analyzed as described previously (27), using a 4000 QTRAP MS/MS system (AB Sciex, Framingham, MA) equipped with the nanoflow ion source TriVersa NanoMate (Advion BioSystems, Ithaca, NY). Ions for ceramide, hexosylceramide, and sphingomyelin were identified by precursor ion scans of *m/z* 264.4 (for ceramide and hexosylceramide) and *m/z* 184.1 (for sphingomyelin) in the positive ion mode and analyzed by Analyst software (version 1.6; AB Sciex).

RESULTS

The TER P182L mutant enzyme exhibits a reduced activity — To investigate the effect of the *P182L* mutation on the *trans*-2-enoyl-CoA reductase activity of the TER enzyme, we first examined the ability of the TER P182L mutant enzyme to complement the growth defect of the yeast *TSC13* mutant deficient in *trans*-2-enoyl-CoA reductase. Since the *TSC13* gene is essential for the growth of yeast (17), we utilized the auxin-inducible degron (AID) system (23) to generate a conditional yeast *TSC13* mutant. Thus, the chromosomal *TSC13* gene was replaced with the *TSC13* gene tagged with tandemly-oriented HA and AID (*TSC13-HA-AID*). As expected, the *TSC13-HA-AID* cells harboring the vector only were not able to grow in the presence of the auxin 3-indolacetic acid (IAA) (Fig. 2*A*) due to the degradation of the Tsc13-HA-AID protein via the ubiquitin-proteasome pathway in response to IAA (Fig. 2*B*). The IAA-induced growth defect of the *TSC13-HA-AID* cells was complemented by the introduction of the plasmid encoding either the wild-type *TER* gene or the *TER P182L* mutant gene; however, the growth of cells expressing the mutant gene was slightly slower than those expressing the wild-type *TER* gene (Fig. 2*A*). In addition, the cellular level of the TER P182L mutant enzyme was found to be much lower (over 5-fold) than that of the wild-type TER enzyme (Fig. 2*B*).

We subsequently performed an *in vitro trans*-2-enoyl-CoA reductase assay using the total membrane fraction from the *TSC13* deletion mutant (*tsc13*Δ) bearing the plasmid encoding either the wild-type *TER* gene or the *TER P182L* mutant gene. In an effort to obtain a similar expression level, each mRNA was transcribed under the control of the weaker *ADH* or strong *GAPDH* promoter, respectively. As a result, the level of the mutant enzyme was increased to about half of the wild-type enzyme level (Fig. 3*A*). An increasing amount of each membrane fraction (*i.e.*, an increasing amount of the 3xFLAG-tagged wild-type/mutant enzyme) was then subjected to the assay using 3-hydroxy[1-^{14}C]palmitoyl-CoA, which is the substrate of 3-hydroxyacyl-CoA dehydratase in the third reaction of the FA elongation cycle (Fig. 1*A*), since the radiolabeled substrate of the TER enzyme, *trans*-2-enoyl-CoA, is not commercially available. The acyl-CoA products were analyzed after hydrolysis to the corresponding FAs. In the absence of the TER enzyme cofactor, NADPH, both membrane fractions accumulated *trans*-2-hexadecenoyl-CoA, some of which were however further converted to palmitoyl-CoA at the higher amount of the membrane fraction (Fig. 3*B*), probably due to the endogenous NADPH

present in the membrane preparation. In both membrane fractions, a nearly identical amount of *trans*-2-enoyl-CoA was produced irrespective of the amount of the membrane fraction, suggesting either that the dehydration reaction by the endogenous yeast 3-hydroxyacyl-CoA dehydratase (Phs1) was saturated under the assay condition or that some 3-hydroxypalmitoyl-CoA was not accessible to the yeast Phs1 enzyme for an unknown reason. In the presence of the cofactor NADPH, the membrane fraction from the yeast *tsc13*Δ mutant carrying the wild-type *TER* gene converted almost all *trans*-2-hexadecenoyl-CoA to palmitoyl-CoA, while, for the yeast *tsc13*Δ mutant carrying the *TER P182L* mutant gene, the degree of the conversion was proportional to the amount of the membrane fraction (Fig. 3, *B* and *C*). The *TER P182L* mutation appears to cause a reduction in the enzyme activity.

The TER P182L mutant enzyme is unstable — It is possible that the lower cellular level of the TER P182L mutant enzyme as compared to the wild-type TER enzyme may be due to its instability; therefore, we conducted a pulse-chase experiment using HEK 293T cells expressing either the 3xFLAG-tagged wild-type *TER* mRNA or the 3xFLAG-tagged *TER P182L* mutant mRNA from the elongation factor 1α promoter. Like in yeast cells, the level of the mutant enzyme was lower than that of the wild-type enzyme (Fig. 4*A*). Cells were pulse-labeled with [^{35}S]Met/Cys and the fate of the labeled enzyme was monitored over time (Fig. 4*B*). The initial amount of the labeled TER P182L mutant enzyme (1 h) was approximately equal to that of the labeled wild-type TER enzyme indicating normal translation of the mutant enzyme. However, during the chase period of 8 h, the amount of the labeled mutant enzyme was reduced to ~20% of the initial level, while the amount of the labeled wild-type enzyme remained little changed (Fig. 4, *B* and *C*). Immunoblotting of each sample used for the pulse-chase experiment showed that the protein level (cold and radiolabeled) was fairly constant for both enzymes (Fig. 4*B*). These results suggest that the *TER P182L* mutation destabilizes the protein.

We also determined the intracellular localization of the TER P182L mutant enzyme using indirect immunofluorescence microscopy. Both the wild-type and mutant enzymes tagged with 3xFLAG displayed a reticular pattern typical for the ER and were merged with the ER marker calreticulin (Fig. 5). The ER localization of the wild-type TER enzyme is consistent with the previous study (6); consequently, the *TER P182L* mutation does not affect the intracellular localization of the enzyme.

The TER P182L mutation has an indirect influence on the third reaction (dehydration of 3-hydroxyacyl-CoA) in the FA elongation cycle — We next analyzed the FA elongation cycle in B-LCLs derived from NSMR patients (homozygous for the *TER P182L* mutation, $TER^{P182L/P182L}$) (19), asymptomatic carriers (heterozygous for the *TER P182L* mutation, $TER^{+/P182L}$), and healthy non-carrier controls ($TER^{+/+}$). The RT-PCR indicated that the expression of the *TER* mRNA was comparable among these B-LCLs (Fig. 6*A*). The total membrane fraction of each B-LCL was incubated with 3-hydroxy[1-^{14}C]palmitoyl-CoA, and the acyl-CoA products were analyzed after conversion to the corresponding FAs (Fig. 6, *B* and *C*). As expected, in the absence of the cofactor NADPH, all the membrane fractions yielded *trans*-2-enoyl-CoA as the only product in ~30% radiochemical yield. In the presence of the cofactor, the $TER^{+/+}$ and $TER^{+/P182L}$ membrane fractions consumed most of *trans*-2-enoyl-CoA producing acyl-CoA in 72 and 61% radiochemical yield, respectively. The $TER^{P182L/P182L}$ membrane fraction, on the other hand, generated only 28% radiochemical yield of acyl-CoA (39% of acyl-CoA produced by the $TER^{+/+}$ membrane fraction) with a significant amount of unreacted *trans*-2-enoyl-CoA.

Since FA elongation is achieved by a repeated cycle of four successive enzyme-catalyzed reactions (Fig. 1*A*), we performed an *in vitro* FA elongation assay to investigate the effect of the *TER P182L* mutation on the overall FA elongation cycle. The total membrane fraction from each B-LCL was incubated with palmitoyl-CoA (the acyl-CoA substrate) and [2-^{14}C]malonyl-CoA (the

two-carbon donor), and the radioactive acyl-CoA products were analyzed as the corresponding radioactive FAs (Fig. 7*A*). Since the first condensation reaction is the rate-limiting step in each round of the FA elongation cycle (4), acyl-CoA was the primary product in all the membrane fractions. In both the *TER*$^{+/+}$ and *TER*$^{+/P182L}$ membrane fractions, 3-hydroxyacyl-CoA was also detected in a small amount but neither 3-ketoacyl-CoA nor *trans*-2-enoyl-CoA was detected. Contrary to our anticipation, the *TER*$^{P182L/P182L}$ membrane fraction accumulated a substantial amount of 3-hydroxyacyl-CoA with only a small amount of *trans*-2-enoyl-CoA (the substrate of the TER enzyme). Similar results were also obtained using HeLa cells with *TER* knockdown (supplemental Fig. 1). The *TER* siRNA caused a reduction in the *TER* mRNA level (supplemental Fig. 1*A*), accompanied by a significant accumulation of 3-hydroxyacyl-CoA and, to a lesser extent, *trans*-2-enoyl-CoA (supplemental Fig. 1, *B* and *C*). Therefore, it seems that the third reaction in the FA elongation cycle was indirectly affected by the impairment of the fourth reaction caused by the reduced enzymatic activity of the TER P182L mutant enzyme.

The levels of C24:1 sphingomyelin and C24:1 ceramide are decreased in the TER$^{P182L/P182L}$ *B-LCL* —Since VLCFAs are components of sphingolipids, the decreased activity of the TER P182L mutant enzyme leads to a reduction in VLCFA synthesis, which may alter the sphingolipid profile in the cell. To test this possibility, we quantitatively analyzed sphingomyelin, ceramide, and hexosylceramide compositions in the *TER*$^{+/+}$, *TER*$^{+/P182L}$, and *TER*$^{P182L/P182L}$ B-LCLs using MS/MS. In all the B-LCLs, C16:0 sphingolipids were the most abundant sphingolipid species, followed by C24:1 and C24:0 sphingolipids (Fig. 8). However, in the *TER*$^{P182L/P182L}$ B-LCL, the levels of C24:1 sphingomylein and C24:1 ceramide were significantly reduced compared to those in the *TER*$^{+/+}$ and *TER*$^{+/P182L}$ B-LCLs (Fig. 8, *A* and *B*). In addition, the levels of C24:0 sphingomyelin and C24:0 ceramide also seemed to be decreased but not statistically significant. Interestingly, there was a concomitant increase in the levels of C16:0 sphingomyelin and C16:0 ceramide. In contrast to sphingomyelin and ceramide, although C16:0 hexosylceramide was significantly increased, no other hexosylceramide showed any noticeable changes in the *TER*$^{P182L/P182L}$ B-LCL (Fig. 8*C*). Nevertheless, these findings indicated that the *TER P182L* mutation also has an influence on the synthesis of sphingolipids.

DISCUSSION

Using yeast and mammalian cells transfected with the *TER P182L* mutant gene, we have revealed that the *TER P182L* mutation reduces the activity and stability of the enzyme (Figs. 3 and 4), which seems to explain the decrease in the apparent TER activity observed in the *TER*$^{P182L/P182L}$ B-LCL (Fig. 6, *B* and *C*). In the predicted membrane topology model of the TER enzyme (Fig. 1*C*), the Pro182 residue is located in the second luminal loop. Due to its cyclic structure, a proline residue confers a local rigidity to the protein backbone and often plays an important role in protein architecture producing turns and bends. Indeed, the Pro182 residue is predicted to constitute a turn structure at the end of a β-strand by a protein secondary structure prediction algorithm (28); accordingly, its substitution with a leucine residue could impair the turn and dislocate the secondary structure, resulting in the reduced enzyme activity and stability.

Each FA elongation cycle is a four-reaction process (Fig. 1*A*), in which the first condensation reaction is the rate-limiting step (4). This is consistent with the results of the FA elongation assay on the B-LCLs showing that the major product was the substrate for the first reaction, acyl-CoA (Fig. 7). Interestingly, in the *TER*$^{P182L/P182L}$ B-LCL and the *TER* siRNA-treated HeLa cells, the substrate for the third reaction, 3-hydroxyacyl-CoA, was the second major product followed by the substrate for the fourth reaction (the TER enzyme-catalyzed reaction), *trans*-2-enoyl-CoA (Fig. 7 and supplemental Fig. 1). A small amount of 3-hydroxyacyl-CoA, but not *trans*-2-enoyl-CoA, was also detected in both the *TER*$^{+/+}$ and *TER*$^{+/P182L}$ B-LCLs (Fig. 7*A*). The substrate for the second reaction,

3-ketoacyl-CoA, was not detected in any of the B-LCLs. This observation implies that the third reaction, dehydration of 3-hydroxyacyl-CoA to *trans*-2-enoyl-CoA, may be the secondary rate-limiting step in the FA elongation cycle and regulated by feedback inhibition of 3-hydroxyacyl-CoA dehydratase by its product accumulation due to the *TER P182L* mutation. It is noteworthy that, in mammals, multiple isozymes exist for both the first and third reactions, in contrast to one enzyme each for the second and fourth reactions, suggesting the importance of the first and third reactions in the FA elongation cycle. Alternatively, since the enzymes involved in the FA elongation cycle are associated as a membrane-bound enzyme complex, any reduction in the TER enzyme level caused by either the *P182L* mutation or siRNA treatment could result in the disruption of the possible interaction of 3-hydroxyacyl-CoA dehydratase with the TER enzyme required for the dehydratase activity and thus the accumulation of its substrate 3-hydroxyacyl-CoA.

The levels of C24:1 sphingomyelin and C24:1 ceramide were significantly decreased in the $TER^{P182L/P182L}$ B-LCL as compared to the $TER^{+/+}$ B-LCL (Fig. 8, *A* and *B*). There was also a decrease in the levels of C24:0 sphingomyelin and C24:0 ceramide, but this was not statistically significant probably due to the small sample size. Ceramide is the common precursor for hexosylceramide and sphingomyelin and therefore it was expected that, similar to C24:1 sphingomyelin, the level of C24:1 hexosylceramide would be decreased in the $TER^{P182L/P182L}$ B-LCL; however, it was found to remain virtually unchanged (Fig. 8*C*). This observation may be explained by the low hexosylceramide content in B-LCL (~1/10 of the sphingomyelin content; data not shown), which could cause measurement deviation. On the other hand, the levels of all three C16:0 sphingolipids were found to be similarly increased in the $TER^{P182L/P182L}$ B-LCL (Fig. 8). Since the TER enzyme is the only *trans*-2-enoyl-CoA reductase, the mutation in the *TER* gene must affect every FA elongation cycle; as a consequence, the effect of the *TER P182L* mutation may become more profound with a progression of the FA elongation cycle (e.g., synthesis of C24 VLCFAs). It is therefore conceivable that, in the $TER^{P182L/P182L}$ B-LCL, the mutation causes a reduction in the production of C24 VLCFAs, which in turn lowers the level of C24 sphingolipids.

In contrast to the *TER* null mutation, which probably leads to embryonic lethality as in the case of the knockout mice for the only 3-ketoacyl-CoA reductase *KAR* gene (18), the *TER P182L* mutation appears to be a weak mutation and affects only neural function in the brain (19). This weak mutation could be consistent with the relatively small changes observed in the level of C24 sphingolipids, which, however, may be enough to harm the nerve system without causing damage to other tissues/organ systems. Myelin plays an important role in the saltatory conduction of action potentials in the nervous system and is enriched in certain lipids, especially C24 sphingolipids (sphingomyelin, galactosylceramide, and sulfatide) (10,12,29). Indeed, mice deficient in C24 ceramide (and hence C24 sphingolipids) are known to exhibit neural defects (30). In this regard, it may be possible that the reduction in C24 sphingolipids as a result of the *TER P182L* mutation could affect neural development contributing to the pathogenesis of NSMR.

In summary, we have identified that the *TER P182L* mutation reduces the activity and stability of the enzyme leading to a decreased level of C24 sphingolipids, an essential component for proper myelin function, in the $TER^{P182L/P182L}$ B-LCL, which may be a part of the pathogenesis of NSMR. We have also found an indication that the third reaction (dehydration of 3-hydroxyacyl-CoA) is likely to be the secondary rate-limiting step in the FA elongation cycle. Future studies will be needed to determine the effect of the *TER P182L* mutation on the brain lipid composition and brain function as well as to reveal the regulatory mechanism of the probable secondary rate-limiting step.

REFERENCES

1. Agbaga, M. P., Mandal, M. N., and Anderson, R. E. (2010) Retinal very long-chain PUFAs: new insights from studies on ELOVL4 protein. *J. Lipid Res.* **51**, 1624-1642
2. Guillou, H., Zadravec, D., Martin, P. G., and Jacobsson, A. (2010) The key roles of elongases and desaturases in mammalian fatty acid metabolism: Insights from transgenic mice. *Prog. Lipid Res.* **49**, 186-199
3. Kihara, A. (2012) Very long-chain fatty acids: elongation, physiology and related disorders. *J. Biochem.* **152**, 387-395
4. Nugteren, D. H. (1965) The enzymic chain elongation of fatty acids by rat-liver microsomes. *Biochim. Biophys. Acta* **106**, 280-290
5. Ohno, Y., Suto, S., Yamanaka, M., Mizutani, Y., Mitsutake, S., Igarashi, Y., Sassa, T., and Kihara, A. (2010) ELOVL1 production of C24 acyl-CoAs is linked to C24 sphingolipid synthesis. *Proc. Natl. Acad. Sci. USA* **107**, 18439-18444
6. Moon, Y. A., and Horton, J. D. (2003) Identification of two mammalian reductases involved in the two-carbon fatty acyl elongation cascade. *J. Biol. Chem.* **278**, 7335-7343
7. Ikeda, M., Kanao, Y., Yamanaka, M., Sakuraba, H., Mizutani, Y., Igarashi, Y., and Kihara, A. (2008) Characterization of four mammalian 3-hydroxyacyl-CoA dehydratases involved in very long-chain fatty acid synthesis. *FEBS Lett.* **582**, 2435-2440
8. Kihara, A., Mitsutake, S., Mizutani, Y., and Igarashi, Y. (2007) Metabolism and biological functions of two phosphorylated sphingolipids, sphingosine 1-phosphate and ceramide 1-phosphate. *Prog. Lipid Res.* **46**, 126-144
9. Hakomori, S. (2000) Traveling for the glycosphingolipid path. *Glycoconj. J.* **17**, 627-647
10. Norton, W. T., and Cammer, W. (1984) Isolation and characterization of myelin. *Myelin*, Pleum Press, New York, NY, pp 147-195
11. Laviad, E. L., Albee, L., Pankova-Kholmyansky, I., Epstein, S., Park, H., Merrill, A. H., Jr., and Futerman, A. H. (2008) Characterization of ceramide synthase 2: tissue distribution, substrate specificity, and inhibition by sphingosine 1-phosphate. *J. Biol. Chem.* **283**, 5677-5684
12. Potter, K. A., Kern, M. J., Fullbright, G., Bielawski, J., Scherer, S. S., Yum, S. W., Li, J. J., Cheng, H., Han, X., Venkata, J. K., Khan, P. A., Rohrer, B., and Hama, H. (2011) Central nervous system dysfunction in a mouse model of FA2H deficiency. *Glia* **59**, 1009-1021
13. Zhang, K., Kniazeva, M., Han, M., Li, W., Yu, Z., Yang, Z., Li, Y., Metzker, M. L., Allikmets, R., Zack, D. J., Kakuk, L. E., Lagali, P. S., Wong, P. W., MacDonald, I. M., Sieving, P. A., Figueroa, D. J., Austin, C. P., Gould, R. J., Ayyagari, R., and Petrukhin, K. (2001) A 5-bp deletion in *ELOVL4* is associated with two related forms of autosomal dominant macular dystrophy. *Nat. Genet.* **27**, 89-93
14. Aldahmesh, M. A., Mohamed, J. Y., Alkuraya, H. S., Verma, I. C., Puri, R. D., Alaiya, A. A., Rizzo, W. B., and Alkuraya, F. S. (2011) Recessive mutations in *ELOVL4* cause ichthyosis, intellectual disability, and spastic quadriplegia. *Am. J. Hum. Genet.* **89**, 745-750
15. Pelé, M., Tiret, L., Kessler, J. L., Blot, S., and Panthier, J. J. (2005) SINE exonic insertion in the *PTPLA* gene leads to multiple splicing defects and segregates with the autosomal recessive centronuclear myopathy in dogs. *Hum. Mol. Genet.* **14**, 1417-1427
16. Muhammad, E., Reish, O., Ohno, Y., Scheetz, T., DeLuca, A., Searby, C., Regev, M., Benyamini, L., Fellig, Y., Kihara, A., Sheffield, V. C., and Parvari, R. Congenital myopathy is caused by mutation of *HACD1*. *Hum. Mol. Genet.*, in press
17. Kohlwein, S. D., Eder, S., Oh, C. S., Martin, C. E., Gable, K., Bacikova, D., and Dunn, T. (2001) Tsc13p is required for fatty acid elongation and localizes to a novel structure at the nuclear-vacuolar interface in *Saccharomyces cerevisiae*. *Mol. Cell. Biol.* **21**, 109-125
18. Rantakari, P., Lagerbohm, H., Kaimainen, M., Suomela, J. P., Strauss, L., Sainio, K., Pakarinen, P., and Poutanen, M. (2010) Hydroxysteroid (17β) dehydrogenase 12 is essential for mouse organogenesis and embryonic survival. *Endocrinology* **151**, 1893-1901

19. Çalişkan, M., Chong, J. X., Uricchio, L., Anderson, R., Chen, P., Sougnez, C., Garimella, K., Gabriel, S. B., dePristo, M. A., Shakir, K., Matern, D., Das, S., Waggoner, D., Nicolae, D. L., and Ober, C. (2011) Exome sequencing reveals a novel mutation for autosomal recessive non-syndromic mental retardation in the *TECR* gene on chromosome 19p13. *Hum. Mol. Genet.* **20**, 1285-1289
20. Paul, S., Gable, K., and Dunn, T. M. (2007) A six-membrane-spanning topology for yeast and *Arabidopsis* Tsc13p, the enoyl reductases of the microsomal fatty acid elongating system. *J. Biol. Chem.* **282**, 19237-19246
21. Fuss, I. J., Kanof, M. E., Smith, P. D., and Zola, H. (2009) Isolation of whole mononuclear cells from peripheral blood and cord blood. *Curr. Protoc. Immunol.* **Chapter 7**, Unit 7. 1.
22. Brachmann, C. B., Davies, A., Cost, G. J., Caputo, E., Li, J., Hieter, P., and Boeke, J. D. (1998) Designer deletion strains derived from *Saccharomyces cerevisiae* S288C: a useful set of strains and plasmids for PCR-mediated gene disruption and other applications. *Yeast* **14**, 115-132
23. Nishimura, K., Fukagawa, T., Takisawa, H., Kakimoto, T., and Kanemaki, M. (2009) An auxin-based degron system for the rapid depletion of proteins in nonplant cells. *Nat. Methods* **6**, 917-922
24. Obara, K., Yamamoto, H., and Kihara, A. (2012) Membrane protein Rim21 plays a central role in sensing ambient pH in *Saccharomyces cerevisiae*. *J. Biol. Chem.* **287**, 38473-38481
25. Kihara, A., and Igarashi, Y. (2002) Identification and characterization of a *Saccharomyces cerevisiae* gene, *RSB1*, involved in sphingoid long-chain base release. *J. Biol. Chem.* **277**, 30048-30054
26. Ogawa, C., Kihara, A., Gokoh, M., and Igarashi, Y. (2003) Identification and characterization of a novel human sphingosine-1-phosphate phosphohydrolase, hSPP2. *J. Biol. Chem.* **278**, 1268-1272
27. Sassa, T., Ohno, Y., Suzuki, S., Nomura, T., Nishioka, C., Kashiwagi, T., Hirayama, T., Akiyama, M., Taguchi, R., Shimizu, H., Itohara, S., and Kihara, A. (2013) Impaired epidermal permeability barrier in mice lacking the Elovl1 gene responsible for very long-chain fatty acid production. *Mol. Cell. Biol.* **33**, 2787-2796
28. Chou, P. Y., and Fasman, G. D. (1974) Prediction of protein conformation. *Biochemistry* **13**, 222-245
29. Ben-David, O., Pewzner-Jung, Y., Brenner, O., Laviad, E. L., Kogot-Levin, A., Weissberg, I., Biton, I. E., Pienik, R., Wang, E., Kelly, S., Alroy, J., Raas-Rothschild, A., Friedman, A., Brugger, B., Merrill, A. H., Jr., and Futerman, A. H. (2011) Encephalopathy caused by ablation of very long acyl chain ceramide synthesis may be largely due to reduced galactosylceramide levels. *J. Biol. Chem.* **286**, 30022-30033
30. Imgrund, S., Hartmann, D., Farwanah, H., Eckhardt, M., Sandhoff, R., Degen, J., Gieselmann, V., Sandhoff, K., and Willecke, K. (2009) Adult ceramide synthase 2 (CERS2)-deficient mice exhibit myelin sheath defects, cerebellar degeneration, and hepatocarcinomas. *J. Biol. Chem.* **284**, 33549-33560

Acknowledgements —The yeast strain for the AID system (BY25598) was provided by the National Bio-Resource Project (NBRP) of the MEXT, Japan. We are grateful to Dr. K. Obara for technical support and Dr. T. Toyokuni for scientific editing of the manuscript.

FOOTNOTES

*****This work was supported by a Grant-in-Aid for Scientific Research (B) (23370057) to AK from the Japan Society for the Promotion of Science (JSPS).

[1]To whom correspondence may be addressed: Faculty of Pharmaceutical Sciences, Hokkaido University, Kita 12-jo Nishi 6-chome, Kita-ku, Sapporo, 062-0812, Japan, Tel.: +81-11-706-3754; Fax: +81-11-706-4900; E-mail: kihara@pharm.hokudai.ac.jp

[2]Department of Biomedical Sciences, College of Life and Health Sciences, Chubu University, 1200 Matsumoto-cho, Kasugai 487-8501, Japan

[3]Department of Human Genetics, University of Chicago, 920 E. 58th Street, Chicago, IL 60637, USA

[4]The abbreviations used are: AID, auxin-inducible degron; B-LCL, B-lymphoblastoid cell line; ER, endoplasmic reticulum; FA, fatty acid; IAA, 3-indoleacetic acid; LCFA, long-chain fatty acid; MS, mass spectrometry; NSMR, non-syndromic mental retardation; SC, synthetic complete; VLCFA, very long-chain fatty acid.

FIGURE LEGENDS

FIGURE 1. The FA elongation cycle and the *TER P182L* mutation. A. The FA elongation cycle consisting of four reactions (condensation, reduction, dehydration, and reduction) and the mammalian enzymes involved in each reaction are illustrated. Each elongation cycle adds two carbons from malonyl-CoA to a growing acyl-CoA chain. B. Nucleotide and amino acid sequences of the TER enzyme and the TER P182L mutant enzyme around the mutation site are presented. C. The predicted membrane topology of the TER enzyme with the P182L mutation site (*) is shown. The prediction was made based on the topology of the yeast and *Arabidopsis* homologs (20).

FIGURE 2. The TER P182L mutant enzyme complements the IAA-induced growth defect of the yeast *TSC13-HA-AID* cells. A and B. Yeast YRF82 cells (*TSC13-HA-AID*) bearing the pAKNF314 (vector), pAB85 (*3xFLAG-TER*), or pAB95 (*3xFLAG-TER P182L*) plasmid were grown in SC-Trp medium at 30 ˚C to full-growth. A. After 1:10 serial dilution, cells were spotted onto plates of SC-Trp and incubated with or without 150 μM IAA (500 mM stock solution in ethanol) at 30 ˚C for 3 days. The dilution factors are indicated above the panel. B. Cells were diluted with SC-Trp medium to A_{600} = 0.3 and incubated at 30 ˚C for 2 h. Cells were then treated with 500 μM IAA (500 mM stock solution in ethanol) or with its solvent ethanol and further incubated at 30 ˚C for 3 h. The total lysate was prepared from each transfected cell population, and the lysate equivalent to A_{600} = 0.2 or 1.0 (x5) units of cells was separated by SDS-PAGE and immunoblotted with anti-FLAG antibody and anti-HA antibody or, to compare protein loading, with anti-Pgk1 antibody.

FIGURE 3. The activity of the TER P182L mutant enzyme is lower than that of the wild-type TER enzyme. A-C. Yeast ABY62 cells (*tsc13*Δ mutant harboring the pAB114 (*3xFLAG-TER*) plasmid) and ABY58 cells (*tsc13*Δ mutant harboring the pAB110 (*3xFLAG-TER P182L*) plasmid) were grown in SC-His medium at 30 ˚C. An increasing amount of the total membrane fraction was subjected to immunoblotting (A) or *in vitro trnas*-2-enoyl-CoA reductase assay (B and C): for cells expressing the 3xFLAG-TER enzyme, 0.625, 1.25, 2,5, 5, and 10 μg and for cells expressing the 3xFLAG-TER P182L mutant enzyme, 1.25, 2,5, 5, 10, and 20 μg (corresponding respectively to 2.5, 5, 10, 20, and 40 ng of the 3xFLAG-TER enzyme as determined by comparison with the 3xFLAG-tagged maltose binding protein standard, which are indicated in the figure). A. Each total membrane fraction was separated by SDS-PAGE and immunoblotted with anti-FLAG antibody or, to compare protein loading, with anti-Pma1 (a plasma membrane protein) antibody. B. Each total membrane fraction was incubated with 1.8 μM 3-hydroxy[1-^{14}C]palmitoyl-CoA (5 nCi) at 37 ˚C for 30 min. After a sequential work-up (see Experimental Procedures), lipids were separated by normal-phase TLC and detected by autoradiography. C. The radioactivities associated with 3-hydroxy-acyl FA, *trans*-2-enoyl FA, and FA in B were quantified by a bioimaging analyzer BAS-2500. Each bar represents the percent of the radioactivity of *trans*-2-enoyl FA (left graph) or FA (right graph) relative to the total radioactivity and the mean ± S.D. of three independent experiments. Statistically significant differences between the activiteies of the TER enzyme and the TER P182L mutant enzyme at the same protein amount are indicated (*p<0.05, **p<0.01; t-test). *trans* FA, *trans*-2-enoyl FA; 3-OH FA, 3-hydroxy FA.

FIGURE 4. The TER P182L mutant enzyme is unstable. A. HEK 293T cells were transfected with the pCE-puro 3xFLAG-1 (vector), pCE-puro 3xFLAG-TER, or pCE-puro 3xFLAG-TER P182L plasmid. Forty-eight hours after transfection, the total lysate (5 μg) prepared from each transfected cell population was separated by SDS-PAGE and subjected to immunoblotting with anti-FLAG antibody or, to demonstrate uniform protein loading, with anti-α-tubulin antibody. B. HEK 293T cells were transfected with the pCE-puro 3xFLAG-TER or pCE-puro 3xFLAG-TER P182L plasmid. Forty-eight hours after transfection, cells were labeled with [^{35}S]Met/Cys at 37 ˚C for 1 h. After changing the medium to remove [^{35}S]Met/Cys, cells were incubated for another 1, 2, 4, and 8 h. At the end of each

incubation time, the total cell lysate was prepared and subjected to immunoprecipitation with anti-FLAG antibody. The precipitate was separated by SDS-PAGE and analyzed by autoradiography and by immunoblotting with anti-FLAG antibody. C. The radioactivities associated with the TER enzyme and the TER P182L mutant enzyme in B were quantified by a bioimaging analyzer BAS-2500. Each value represents the percentage of the radioactivity of the TER enzyme or the TER P182L mutant enzyme relative to its radioactivity at the 1-h chase point and the mean ± S.D. of three independent experiments. Statistically significant differences between the radioactivities of the TER enzyme and the TER P182L mutant enzyme at the same chase point are indicated (*$p < 0.05$, **$p < 0.01$; *t* test).

FIGURE 5. The TER P182L mutant enzyme is localized in the ER. HeLa cells were transfected with the pCE-puro 3xFLAG-1 (vector), pCE-puro 3xFLAG-TER, or pCE-puro 3xFLAG-TER P182L plasmid. Forty-eight hours after transfection, the transfected cells were fixed with formaldehyde and permeabilized with 0.1% Triton X-100. The cells were stained with anti-FLAG antibody (red, left panel), anti-calreticulin antibody (green, middle panel), and the DNA-staining reagent DAPI (blue, right panel). Calibration bar, 10 μm.

FIGURE 6. The *TER*$^{P182L/P182L}$ B-LCL exhibits lower *trans*-2-enoyl-CoA reductase activity compared to the *TER*$^{+/+}$ B-LCL. A-C. Three B-LCL clones were used for each *TER* genotype: for *TER*$^{+/+}$, clone CONT_1 (lane 1 in A and B), clone CONT_2 (lane 2 in A and B), and clone CONT_3 (lane 3 in A and B); for *TER*$^{+/P182L}$, clone NSMRC_1 (lane 4 in A and B), clone NSMRC_2 (lane 5 in A and B), and clone NSMRC_3 (lane 6 in A and B); and for *TER*$^{P182L/P182L}$, clone NSMR_1 (lane 7 in A and B), clone NSMR_2 (lane 8 in A and B), and clone NSMR_3 (lane 9 in A and B). A. The *TER* and *GAPDH* cDNAs were amplified by RT-PCR from the total RNA prepared from each B-LCL clone using a specific primer. The amplified fragments were separated by agarose gel electrophoresis and stained with ethidium bromide. B. The total membrane fraction (20 μg) prepared from each B-LCL clone was incubated with 1.8 μM 3-hydroxy[1-^{14}C]palmitoyl-CoA (5 nCi) in the presence or absence of 1 mM NADPH at 37 ˚C for 30 min. After a sequential work-up (see Experimental Procedures), lipids were separated by normal-phase TLC and detected by autoradiography. C. The radioactivities associated with 3-hydroxy-acyl FA, *trans*-2-enoyl FA, and FA in B were quantified by a bioimaging analyzer BAS-2500. Each bar represents the percent of the radioactivity of *trans*-2-enoyl FA or FA relative to the total radioactivity and the mean ± S.D. of three clones. Statistically significant differences are indicated (*p<0.05, **p<0.01; t-test). PL, P182L; *trans* FA, *trans*-2-enoyl FA; 3-OH FA, 3-hydroxy FA.

FIGURE 7. 3-Hydroxyacyl-CoA is accumulated in the *TER*$^{P182L/P182L}$ membrane in the FA elongation assay. A. Three B-LCL clones were used for each *TER* genotype: for *TER*$^{+/+}$, clone CONT_1 (lane 1), clone CONT_2 (lane 2), and clone CONT_3 (lane 3); for *TER*$^{+/P182L}$, clone NSMRC_1 (lane 4), clone NSMRC_2 (lane 5), and clone NSMRC_3 (lane 6); and for *TER*$^{P182L/P182L}$, clone NSMR_1 (lane 7), clone NSMR_2 (lane 8), and clone NSMR_3 (lane 9). The total membrane fraction (20 μg) prepared from each B-LCL clone was incubated with 20 μM palmitoyl-CoA and 27.3 μM [2-^{14}C]malonyl-CoA (0.075 μCi) at 37 ˚C for 30 min. After a sequential work-up (see Experimental Procedures), lipids were separated by normal-phase TLC and detected by a bioimaging analyzer BAS-2500. B. The radioactivities associated with 3-hydroxy-acyl FA, *trans*-2-enoyl FA, and FA in A were quantified by a bioimaging analyzer BAS-2500. Each bar represents the percent of the radioactivity of each lipid relative to the total radioactivity and the mean ± S.D. of three independent experiments. Statistically significant differences are indicated (*p<0.05; *t*-test). *trans* FA, *trans*-2-enoyl FA; 3-OH FA, 3-hydroxy FA.

FIGURE 8. C24:1 sphingomyelin and C24:1 ceramide are decreased in the *TER*$^{P182L/P182L}$ B-LCL. Lipids were extracted from multiple cells for each B-LCL clone: for *TER*$^{+/+}$, clones CONT_1,

CONT_2, and CONT_3; for $TER^{+/P182L}$, clones NSMRC_1, NSMRC_2, NSMRC_3, and NSMRC_4; and for $TER^{P182L/P182L}$, NSMR_1, NSMR_2, NSMR_3, and NSMR_4. Sphingomyelin (A), ceramide (B), and hexosylceramide (C) compositions were identified by a 4000 QTRAP MS/MS system and analyzed by Analyst software. Each bar represents the percent of the amount of each sphingolipid species relative to the total amount of the each corresponding sphingolipid and the mean ± S.D. from three or four clones. Statistically significant differences are indicated (*$p < 0.05$, **$p < 0.01$; *t* test).

Figure 1

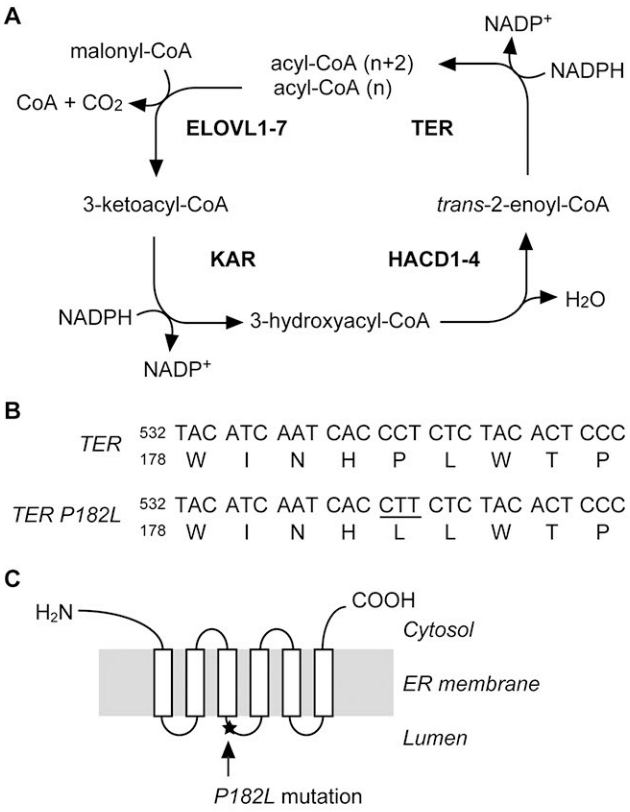
A
malonyl-CoA
CoA + CO2
ELOVL1-7
acyl-CoA (n+2)
acyl-CoA (n)
NADP+
NADPH
TER
3-ketoacyl-CoA
trans-2-enoyl-CoA
KAR
HACD1-4
NADPH
NADP+
3-hydroxyacyl-CoA
H2O
B
TER
532 TAC ATC AAT CAC CCT CTC TAC ACT CCC
178 W I N H P L W T P
TER P182L
532 TAC ATC AAT CAC CTT CTC TAC ACT CCC
178 W I N H L L W T P
C
H2N
COOH
Cytosol
ER membrane
Lumen
P182L mutation

Figure 2

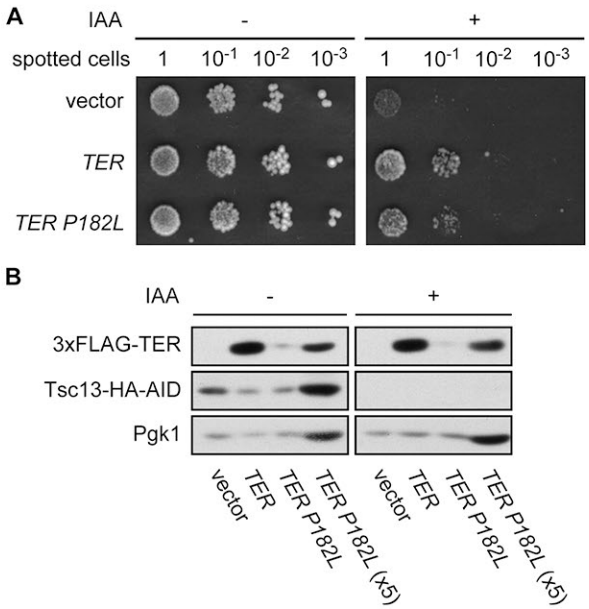
A
IAA
-
+
spotted cells
1
10-1
10-2
10-3
1
10-1
10-2
10-3
vector
TER
TER P182L
B
IAA
-
+
3xFLAG-TER
Tsc13-HA-AID
Pgk1
vector
TER
TER P182L
TER P182L (x5)
vector
TER
TER P182L
TER P182L (x5)

Figure 3

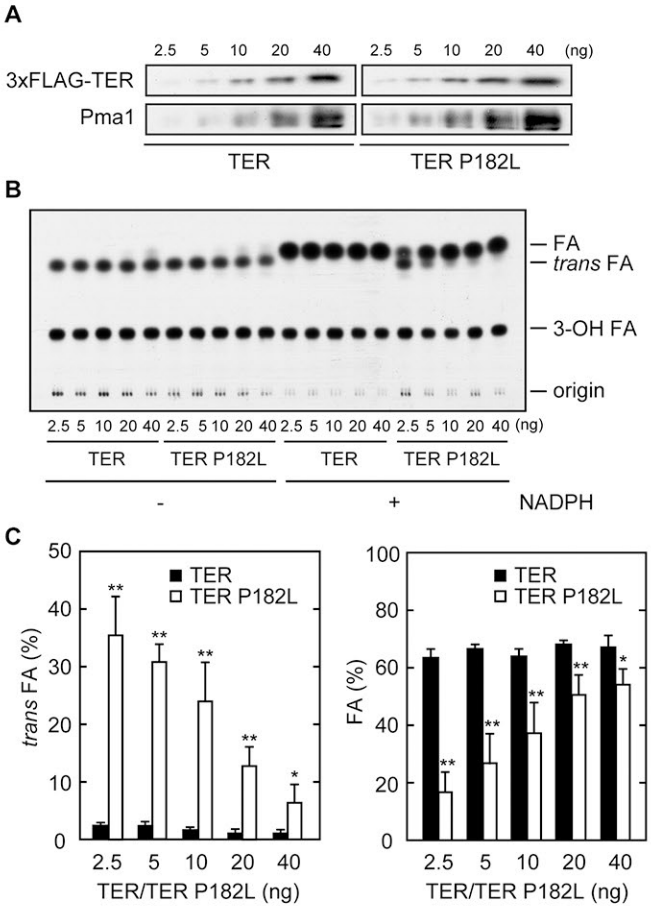
A
2.5 5 10 20 40 2.5 5 10 20 40 (ng)
3xFLAG-TER
Pma1
TER
TER P182L
B
FA
trans FA
3-OH FA
origin
2.5 5 10 20 40 2.5 5 10 20 40 2.5 5 10 20 40 2.5 5 10 20 40 (ng)
TER
TER P182L
TER
TER P182L
-
+
NADPH
C
TER
TER P182L
trans FA (%)
FA (%)
2.5 5 10 20 40
TER/TER P182L (ng)

Figure 4

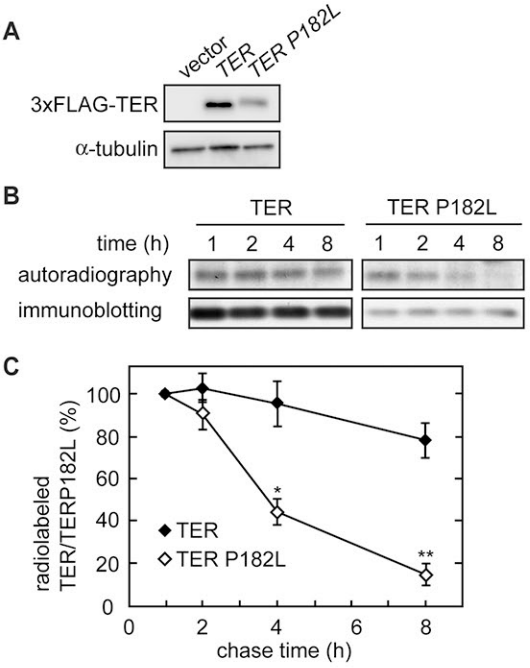
A
vector
TER
TER P182L
3xFLAG-TER
α-tubulin
B
TER
TER P182L
time (h)
1 2 4 8
1 2 4 8
autoradiography
immunoblotting
C
radiolabeled TER/TERP182L (%)
100
80
60
40
20
0
TER
TER P182L
*
**
0 2 4 6 8
chase time (h)

Figure 5

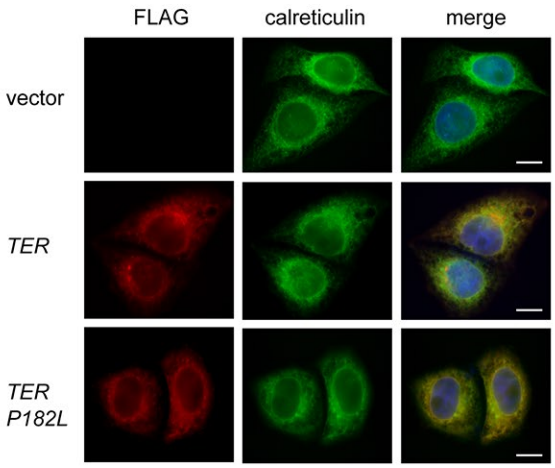

Figure 6

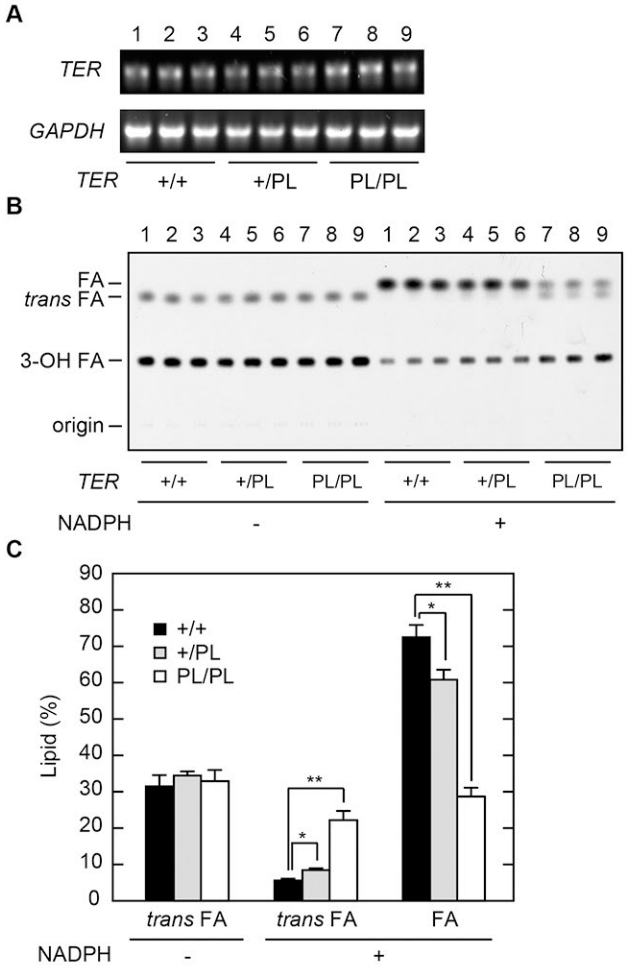
A
1 2 3 4 5 6 7 8 9
TER
GAPDH
TER +/+ +/PL PL/PL
B
1 2 3 4 5 6 7 8 9 1 2 3 4 5 6 7 8 9
FA
trans FA
3-OH FA
origin
TER +/+ +/PL PL/PL +/+ +/PL PL/PL
NADPH - +
C
Lipid (%)
90
80
70
60
50
40
30
20
10
0
+/+
+/PL
PL/PL
**
*
**
*
trans FA
trans FA
FA
NADPH - +

Figure 7

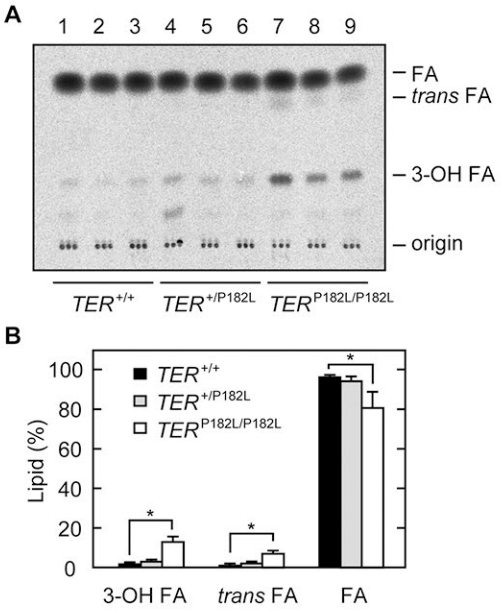
A
1 2 3 4 5 6 7 8 9
FA
trans FA
3-OH FA
origin
TER+/+
TER+/P182L
TERP182L/P182L
B
Lipid (%)
100
80
60
40
20
0
TER+/+
TER+/P182L
TERP182L/P182L
*
*
*
3-OH FA
trans FA
FA

Figure 8

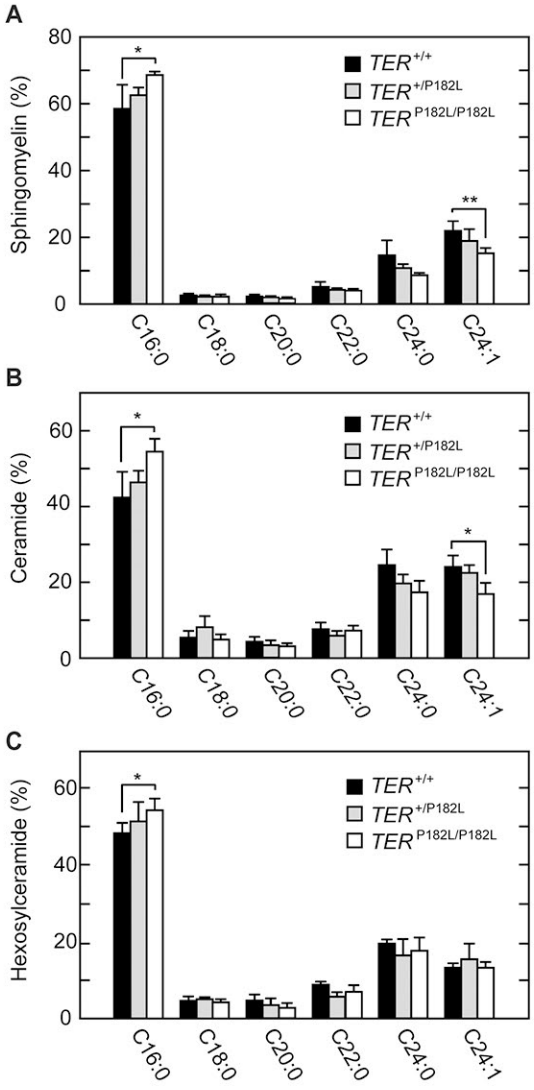
A
Sphingomyelin (%)
80
60
40
20
0
*
**
TER+/+
TER+/P182L
TERP182L/P182L
C16:0
C18:0
C20:0
C22:0
C24:0
C24:1
B
Ceramide (%)
60
40
20
0
*
*
TER+/+
TER+/P182L
TERP182L/P182L
C16:0
C18:0
C20:0
C22:0
C24:0
C24:1
C
Hexosylceramide (%)
60
40
20
0
*
TER+/+
TER+/P182L
TERP182L/P182L
C16:0
C18:0
C20:0
C22:0
C24:0
C24:1